energies

MDPI

Article

Development of Deep Learning Simulation and Density Functional Theory Framework for Electrocatalyst Layers for PEM Electrolyzers

Jaydev Zaveri [1], Shankar Raman Dhanushkodi [1,*], Michael W. Fowler [2], Brant A. Peppley [3], Dawid Taler [4], Tomasz Sobota [4] and Jan Taler [5,*]

[1] Dhanushkodi Research Group, Department of Chemical Engineering, Vellore Institute of Technology, Katpadi, Vellore 632014, Tamil Nadu, India
[2] Department of Chemical Engineering, University of Waterloo, Waterloo, ON N2L3G1, Canada; mfowler@uwaterloo.ca
[3] Department of Chemical Engineering, Queens University, Kingston, ON K7L 3L6, Canada; peppley@queensu.ca
[4] Department of Thermal Processes, Faculty of Environmental Engineering and Energy, Cracow University of Technology, 31-864 Cracow, Poland
[5] Department of Energy, Cracow University of Technology, 31-864 Cracow, Poland
* Correspondence: shankarraman.d@vit.ac.in (S.R.D.); jan.taler@pk.edu.pl (J.T.)

Abstract: The electrocatalyst layers (ECLs) in polymer electrolyte membrane (PEM) electrolyzers are fundamentally comprised of IrOx catalysts, support material, and an ionomer. Their stability is critically dependent on structure and composition, necessitating a thorough understanding of ionization potential and work function. We employ Density Functional Theory (DFT) to determine the ionization states of ECLs and to optimize their electronic properties. Furthermore, advanced deep learning simulations (DLSs) significantly enhance the kinetic and transport behaviors of these layers. This work integrates DFT and DLS to elucidate the characteristics of ECLs within PEM electrolyzer cells. We strategically utilize DFT to refine catalyst molecules and assess their electronic properties, while DLS is employed to predict the potential energy of support molecules in the catalyst layers. We establish a clear relationship between the energy and geometry of IrOx molecules. The DFT-DLS framework robustly calculates potential energy and reaction coordinates, effectively bridging theoretical computations with the dynamic behavior of molecules in catalyst layers. We validate our model by comparing it with the experimental polarization curve of the IrOx-based anode catalyst layer in a functioning electrolyzer. The observed Tafel slope and exchange current density unequivocally confirm that the oxygen evolution reaction (OER) occurs through a well-defined electrochemical pathway, with oxygen generation proceeding according to the charge transfer mechanism predicted by the DFT-DLS framework.

Keywords: computational chemistry; deep learning simulations; artificial neural network; density functional theory; electrocatalyst

Academic Editors: Fernando Sánchez Lasheras, Jean Marie Vianney Nsanzimana and Theophile Niyitanga

Received: 7 January 2025
Revised: 6 February 2025
Accepted: 18 February 2025
Published: 20 February 2025

Citation: Zaveri, J.; Dhanushkodi, S.R.; Fowler, M.W.; Peppley, B.A.; Taler, D.; Sobota, T.; Taler, J. Development of Deep Learning Simulation and Density Functional Theory Framework for Electrocatalyst Layers for PEM Electrolyzers. *Energies* **2025**, *18*, 1022. https://doi.org/10.3390/en18051022

1. Introduction

Hydrogen generated through water electrolysis stands as a pivotal carbon-free energy source, essential for decarbonizing industries such as ammonia production and steel manufacturing. Polymeric Exchange Membrane Water Electrolyzers (PEMWEs) are at the forefront of this innovation, efficiently splitting water into hydrogen and oxygen to enable

green hydrogen production for industrial applications. The U.S. Department of Energy (DOE) is actively working to enhance the efficiency and cost-effectiveness of electrolysis, aiming for a 30% reduction in electrolyzer costs by 2030 and achieving efficiency levels exceeding 80% for large-scale systems [1]. Green electrolysis, powered by renewable energy, plays a crucial role in promoting global sustainability by significantly reducing greenhouse gas emissions and accelerating the transition to clean energy. Within PEMWE cells, both the oxygen evolution reaction (OER) and hydrogen evolution reaction (HER) occur simultaneously at the electrodes (Figure 1), producing gas [2]. To elevate the performance of PEMWEs, it is imperative to understand the electronic structure of the electrodes and the mechanisms of interfacial electron transfer.

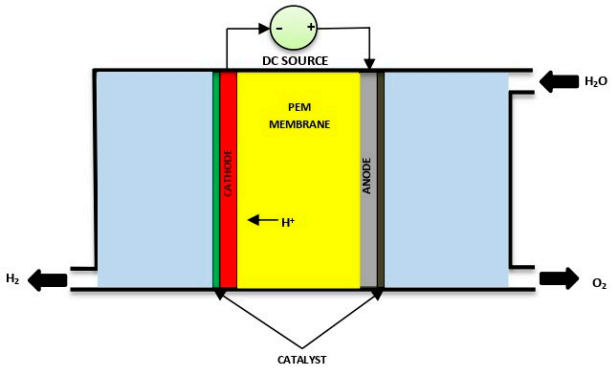

Figure 1. Schematics of the PEM electrolyzer.

$$H_2O \rightarrow O_2 + 4H^+ + 4e^- \quad \text{(OER)} \quad \text{E} = -1.23\ \text{V} \tag{1}$$

$$4\ H^+ + 4e^- \rightarrow 2H_2 \quad \text{(HER)} \quad \text{E} = 0\ \text{V} \tag{2}$$

The electrocatalyst layers (ECLs) in a polymer electrolyte membrane electrolyzer consist of IrOx catalysts, carbon support materials, and an ionomer. Selecting the optimal electrocatalysts is essential for enhancing the energy conversion efficiency of water splitting, which generates hydrogen and oxygen, enabling the production of sustainable, environmentally friendly fuels [3]. Green electrolysis relies on efficient electron transfer across multiple interfaces within the electrolyzer components to produce clean fuels. Unlike industrial catalysts that typically affect reaction rates and selectivity, electrocatalysts in PEMWEs are specifically designed to control the kinetics of water decomposition via the applied voltage, or overpotential (as described in Equations (1) and (2), which govern the reaction rate and material requirements [4]. Additionally, mass transport effects influence current flow, creating both challenges and opportunities for improving performance, which has driven research into three-dimensional electrode materials to surpass traditional two-dimensional surfaces. Effective electrocatalyst design requires optimization of structural properties, as the efficiency of redox reactions depends on the careful selection of both electrocatalysts and support materials. Common HER cathode catalysts include ruthenium, palladium, and platinum, while IrOx, particularly IrO_2, is the preferred OER anode catalyst due to its excellent corrosion resistance, activity, and stability [5]. Despite the promise of binary compositions like IrO_2–RuO_2 in electrochemical activity and stability, their durability under operational conditions remains insufficient for large-scale use. Issues like particle agglomeration, catalyst dissolution, and migration within the ECL degrade electrode polarization and durability, necessitating optimization of IrO_2 to reduce costs. Understanding the OER mechanism at the atomic level is crucial, and Density Functional Theory (DFT) can provide insights by calculating the electronic structure and energy states of materials at the atomic scale. DFT allows for the determination of adsorption energies, reaction energies, and electronic density of states, all critical for understanding catalytic activity [6,7]. Research

has shown that the IrOx (100) surface is more active than the (110) surface for OER, but no studies have yet modeled the redox processes at IrOx surfaces under real operating conditions in electrolyzer cells. Calculating atomistic descriptors for the hydrogen evolution reaction (HER) and oxygen evolution reaction (OER) at the water–electrode interface poses a significant challenge. These descriptors—such as adsorption energies, bond strengths, and electronic properties including work function and ionization potential—are critical for understanding how the catalyst surface interacts with water molecules [8]. Accurately determining these properties necessitates detailed quantum mechanical simulations to capture the complex behaviors of water and catalyst molecules during redox reactions. Guided by Equations (1) and (2), which elucidate the energetics of electron transfer and molecule adsorption, achieving precise atomistic descriptors is essential for optimizing electrode materials and enhancing reaction kinetics [9]. Addressing this challenge is crucial for boosting the efficiency and effectiveness of PEMWE technology and achieving the performance targets established by initiatives like the U.S. Department of Energy's hydrogen electrolysis research goals. This highlights the need for further DFT analysis in electrocatalyst development for electrolyzer cells, as accurate simulations are crucial for optimizing materials and improving overall system performance. Both structured and unstructured data are available from DFT [10–13] and can be effectively used to predict the property and performance of the catalyst [14]. Recent challenges reported in this area are given in Table 1.

Table 1. Research challenges related to DFT analysis of electrocatalysts.

Challenge Area	Summary	Impact of DFT Modeling	Properties That Can Be Extracted	Identified Challenges	References
Preparation Method Variability	Inconsistencies in catalyst properties due to synthesis methods.	Models surface properties and predicts effects of preparation methods.	Surface energy, adsorption, and stability.	Difficulty modeling due to preparation effects; lack of experimental data.	[15,16]
Catalyst Selection	Balancing cost, activity, and durability under harsh conditions.	Evaluates electronic properties and stability for optimal selection.	Binding energy, band gap, DOS, and activity.	Modeling stability under extreme conditions; long-term degradation.	[17–21]
3D Electrode Design	Optimizing overpotential and reaction kinetics for HER/OER.	Simulates 3D structures to predict geometric effects.	Overpotential, current density, and intermediates.	Computational limits; difficulty with complex geometries.	[22–27]
Computational Cost	High-level methods are expensive, limiting large-scale applications.	Simplifies large systems due to high costs.	Computational cost and energy convergence.	Need for approximations; time-intensive for large systems.	[28–32]
Functional Selection	Choosing accurate exchange-correlation functionals for predictions.	Relies on functional groups for property prediction.	Functional accuracy, band gap, and energetics.	Inaccuracies in predictions; errors in band gaps.	[28]

Table 1. *Cont.*

Challenge Area	Summary	Impact of DFT Modeling	Properties That Can Be Extracted	Identified Challenges	References
System Sensitivity	Sensitive to initial geometry, causing convergence challenges.	Requires advanced optimization for reliable predictions.	Total energy and optimized geometries.	Convergence difficulty; sensitivity to initial conditions.	[33–36]
Complex Systems Modeling	Struggles with multi-layer systems and interfacial behaviors.	Hybrid/multi-scale models improve accuracy.	Interfacial energies, binding, and charge transfer.	Capturing interfacial interactions and long-range effects.	[33]
Data Integration	Limited experimental data hinder model validation, especially for alloys.	Requires experimental data for validation.	Adsorption energy and activation energy.	Lack of experimental data for alloys; validation challenges.	[37,38]
Electron Transfer	Modeling electron transfer in multi-step reactions (e.g., OER and HER).	Models electron density changes and transfer pathways.	Electron density, charge transfer, and redox states.	Difficulty modeling electron delocalization and transfer pathways.	[39,40]
Binding Energy and Stability	Calculating binding energies and assessing durability under stress.	Predicts stability and durability under operational stress.	Binding energy, adsorption, and stability.	Complexity in multi-phase systems; long-term stability challenges.	[35]
Core–Shell and 3D Modeling	Modeling core–shell catalysts and 3D electrodes for OER/HER efficiency.	Predicts core–shell behavior and geometric effects.	Surface structure and catalytic activity.	Handling complex core–shell geometries; multi-scale challenges.	[36,37]
Empirical Data Limitations	Limited experimental data on atomic interactions in mixed oxide catalysts.	Requires experimental validation for accurate predictions.	Atomic interactions and polarization.	Lack of sufficient experimental data; limitations in modeling mixed oxides.	[38,39]
Immediate Need/Research Gap	Advanced quantum modeling and core–shell structures are promising but costly.	Multi-scale simulations and quantum methods to overcome limitations.	Band gap, intermediates, and quantum effects.	High computational cost and time; refinement needed for core–shell behavior.	

Machine learning (ML) and deep learning (DL) are transforming electrocatalysis by providing advanced tools for developing efficient catalysts. While both techniques are based on similar principles, they differ in complexity. ML uses sophisticated algorithms to analyze data patterns and make rapid predictions about material properties, linking them

to catalyst performance in key reactions like oxygen reduction [40–42]. It can quickly assess large databases, identifying promising candidates without relying on time-consuming methods like Density Functional Theory (DFT). Conversely, DL employs complex neural networks to extract intricate patterns from high-dimensional datasets. It is particularly effective at analyzing extensive data from simulations and experiments, using techniques like convolutional and recurrent neural networks. DL has shown remarkable success, achieving 92% accuracy in predicting intermediates for oxygen evolution, highlighting its effectiveness in managing complex data relationships. Both machine learning (ML) and deep learning (DL) bring significant advantages to electrocatalysis. They enhance speed and efficiency while alleviating the computational demands of traditional methods like Density Functional Theory (DFT), which require lengthy calculations for each material. ML rapidly predicts catalyst performance, enabling fast screening of large databases for effective materials, such as those used in oxygen reduction reactions (ORRs). In contrast, DL excels in optimizing complex datasets and reaction mechanisms, refining catalyst performance in real-world applications. DL not only improves accuracy but also handles non-linear relationships in data, which are vital for predicting outcomes in intricate systems. Recent studies show DL's capability to predict adsorption energies for over 100 materials with a mean absolute error below 0.05 eV—an important factor in catalyst optimization [40–43]. Both ML and DL facilitate the swift discovery of new materials by analyzing unstructured datasets and uncovering hidden correlations. This has led to breakthroughs like identifying novel nickel-based alloys for oxygen evolution reactions (OERs).

As the data complexity in electrocatalysis grows, DL's role becomes increasingly essential. While DFT remains powerful, its computational intensity can be cumbersome. In contrast, ML and DL can quickly analyze large datasets and predict material properties effectively. For instance, DL has helped reduce the number of necessary DFT calculations for CO_2 reduction screening by up to 50%. This synergy between DL and DFT accelerates discovery and enhances accuracy, making DL a critical tool for advancing efficient and stable electrocatalysts. Beyond optimizing catalysts, ML and DL significantly enhance support materials in electrocatalysis. For instance, graphene has proven to be an effective support for platinum (Pt) catalysts, boosting their stability and activity. Quantitative Structure–Activity Relationship (QSAR) models, integrated with ML, are now used to accurately predict the performance of new oxygen reduction reaction (ORR) catalysts, such as metal–nitrogen–carbon composites. Additionally, Graph Neural Networks (GNNs) can predict adsorption energies exceptionally well (with a mean absolute error under 0.05 eV), facilitating swift screening of catalysts for CO_2 reduction. The integration of ML, DL, and Density Functional Theory (DFT) is revolutionizing electrocatalysis by expediting the discovery and optimization of new catalysts and support materials. These sophisticated computational tools enable researchers to investigate new materials and reaction mechanisms more efficiently and precisely [42–44]. As these technologies advance, they will be vital in developing sustainable energy solutions, particularly in creating more effective and durable electrocatalysts and support materials for various energy conversion processes. In summary, advancements in ML can filter extensive molecular libraries, helping discover materials with tailored properties for applications ranging from energy storage to organic electronics.

Deep learning techniques are increasingly complementing DFT in predicting material properties, delivering rapid and accurate assessments essential for material discovery. Various models like convolutional neural networks (CNNs), recurrent neural networks (RNNs), GNNs, and transformer-based architectures adeptly capture complex molecular interactions. GNNs excel in predicting electronic properties by modeling atomic structures as graphs, while transformer models effectively forecast frontier orbital energies and

reaction mechanisms [45–49]. When trained on DFT-calculated datasets, these models can rapidly estimate critical properties, enabling efficient screening of large molecular libraries to identify candidates with desirable optoelectronic, catalytic, and mechanical characteristics. We need a benchmark model to predict the potential energy (label for the DL model) of a molecule based on various input parameters (features for the DL model) such as the nuclear coordinates and dipole moment in 3D space, the magnetic tensor, Mulliken charge, bond length, and electronegativity of the atom [48]. The present study aims to develop a universal model that can be used in new catalyst material development, which can match the structure–property–performance of iridium oxide catalysts. The further model must have the ability to assess the various dopants that would increase the catalyst's efficiency and help reduce their cost. The research needs on DFT and DLS are provided in Table 2. Thereby, we identify a research gap that can be addressed by integrating the DFT-DLS framework. To expedite the framework, the following objectives are defined:

- Performing the baseline DFT analysis to assess the molecular stability of the known electrocatalyst molecule
- Obtaining the optimum bond length and bond angle with HOMO and LUMO structure for the same molecules
- Extending DFT to study the OER pathway and develop a PES plot, which can be further used to identify the reaction pathway and reaction rate and understand reaction dynamics.
- Correlating the OER data obtained from the PEM electrolyzer with the reference electrode cell to DFT data obtained from the simulation
- Developing deep learning model to assess the predictive maintenance for the support molecules of the electrocatalyst

Table 2. Rationale for choosing DFT against other methods [50–58] to establish the DFT-DLS framework.

	Key Description	Applications	Accuracy	Can it Predict Redox η?	Can it Predict Catalytic Activity?	Limiations
Ab initio Method	Predicts molecular properties by solving the Schrödinger equation.	Design and optimize the electrocatlyst	High	Yes	Yes, but limited for large catalysts.	Slow convergence for large systems.
Schrödinger Equation	Describes electron interactions.	Electronic structure and quantum chemistry	High	Yes	No. Inadequate for simulating large catalytic cycles.	Inefficient for large ones.
Hamiltonian Operator	Describes system's energy through kinetic and potential energy.	Quantum mechanical simulations	High	Yes	No	Computationally expensive and inefficient for large ones.

Table 2. *Cont.*

	Key Description	Applications	Accuracy	Can it Predict Redox η?	Can it Predict Catalytic Activity?	Limiations
DFT (Density Functional Theory)	Calculates electronic structure considering electron density, widely used for large systems.	Molecular simulations and material science	High	Yes	Yes. Commonly used in identifying reaction pathways.	Efficient for medium-large systems, but slow and costly for large systems.
Kohn–Sham Equation	Describes electronic structure using self-consistent effective potential.	Material modeling and reaction pathways	High for moderate-sized systems.	Yes	Yes. Effective for simulating reaction steps during catalysis.	Good for the charge distribution analysis alone.
Potential Energy Surface (PES)	Uses 3D plot showing potential energy as a function of atomic coordinates to assess the reaction dynamics.	Reaction pathway analysis and molecular dynamics	High for small-to-medium-sized systems.	Yes	Yes	Useful for the analysis of reaction steps, but is slow and costly for larger systems.
Deep Learning Simulation	Uses artificial neural networks (ANNs) to predict properties based on training data.	Large dataset property prediction	High	Yes	Yes	Can predict redox efficiently after training.

2. Theory

In this section, we assess the methods and theories adopted to model the DFT (Sections 2.1–2.4) and the deep learning simulations (Section 2.5).

2.1. Theory Related to Performing the Baseline DFT and Assessing the Molecular Stability of the Known Electrocatalyst Molecule

Both DFT and deep learning are efficient for predicting redox behavior, but methods like ab initio and Schrödinger equations are too slow for large systems (Table 2). Both DFT and Kohn–Sham equations are widely used to simulate catalytic reactions, but they are computationally expensive for large systems. Deep learning is efficient post-training for catalytic predictions. A detailed table is given to justify the rationale for choosing the DFT and DLS to address the objectives.

2.2. Basic DFT Equations Applied to Compute the Structure of the Electrocatalyst Molecule

It is a computational method used to calculate the electronic structure of atoms and molecules by considering electron density. It is based on the two Hohenberg–Kohn theorems, which state that its electron density uniquely determines a system's electronic ground-state properties and that a trial electron density must give an energy greater than or equal to the true energy [50–53].

$$E = E_o[p_o(r)] \tag{3}$$

where E is the ground-state energy and $p_o(r)$ is the density functional. The DFT approach reduces the problem from 3N to N electrons. A collection of non-interacting electrons (given by the Kohn–Sham equation) in an effective potential that can be derived self-consistently from the electron density. This is used to model the system in the DFT approach. The effective potential includes the external potential due to the nuclei and any other external fields and an exchange-correlation potential that considers the effects of electron–electron interactions. The Kohn–Sham equation, which describes the electronic structure of a molecule or material, is as follows:

$$\left[-(1/2)\nabla 2 + v_{eff}(r)\right]\psi_i(r) = \varepsilon_i\psi_i(r) \tag{4}$$

where ψ_i (r) represents the ith single-particle wave function, ε_i is the corresponding energy eigenvalue, and υ_eff represents the effective potential that includes both the external and the exchange-correlation potential. The exchange-correlation potential is a function of the electron density, which is determined self-consistently by wave functions.

2.3. DFT Equations to Generate Potential Energy Surface (PES) Plot

It is a three-dimensional diagram that depicts a system's potential energy as a function of the coordinates of the atoms or molecules that make up the system [59,60]. Furthermore, it demonstrates how a molecule's potential energy varies when its atoms move above each other. It also aids in analyzing chemical reactions and molecular dynamics by revealing the energy hurdles that must be surmounted for a reaction [52]. The equations governing the PES depend on the specific interaction potential being considered. The Lennard–Jones potential can be used to explain PES for a simple two-body interaction.

$$V(r) = 4{\cdot}\varepsilon{\cdot}\left[\left(\frac{\sigma^{12}}{r}\right) - \left(\frac{\sigma^{6}}{r}\right)\right] \tag{5}$$

where r represents the distance between the two atoms, ε is the good depth, and σ is the distance at which the potential energy is zero. By analyzing this equation, we can predict the most stable structures of a molecule, the transition states involved in a reaction, and the activation energy required for a reaction to proceed. The negative gradient of the potential energy then gives the force between the two atoms:

$$F(r) = -\frac{dV(r)}{dr} = 24{\cdot}\frac{\varepsilon}{r}{\cdot}\left[2{\cdot}\left(\frac{\sigma^{12}}{r}\right) - \left(\frac{\sigma^{6}}{r}\right)\right] \tag{6}$$

The PES is often depicted as a multidimensional surface, where each dimension corresponds to a different coordinate (e.g., bond lengths, bond angles, dihedral angles, etc.) for a more complicated system, like a polyatomic molecule. In this instance, the equations regulating the PES are more intricate and depend on the particular form of the interaction

potential used. PES for polyatomic molecules can be given by molecular mechanics force fields, which involve a combination of bonded and nonbonded interactions between atoms.

$$E = E_{bond} + E_{angle} + E_{\text{dihedral}} + E_{\text{vdw}} + E_{\text{elec}} \quad (7)$$

where E_{bond}, E_{angle}, $E_{dihedral}$, E_{vdw}, and E_{elec} correspond to the energy contributions from bond stretching, angle bending, torsion (dihedral) rotation, van der Waals interactions, and electrostatic interactions, respectively.

2.4. Correlating the OER of the PEM Electrolyzer with DFT Data

To establish a robust correlation between Oxygen Evolution Reaction (OER) data from a PEM electrolyzer with a reference electrode cell and Density Functional Theory (DFT) simulations, a comprehensive approach is needed. Experimental data must be collected by varying operational conditions, such as voltage and current density, in the PEM electrolyzer while using a reference electrode to accurately measure the electrochemical potential, ensuring precise data free from interference [61]. Key metrics like overpotentials, current densities, and Tafel slopes are required to assess the OER performance. Concurrently, DFT simulations must be performed to investigate the catalyst's electronic structure and reaction pathways, focusing on energy barriers and the binding energies of key intermediates (e.g., OH and O). These computational insights can then be correlated with experimental data, comparing overpotentials and energy barriers to confirm that lower overpotentials correspond with lower energy barriers, indicating more efficient catalysts. Current densities were compared with reaction rate constants derived from DFT to ensure faster kinetics align with experimental observations.

2.5. Deep Learning Simulation (DLS) for Electrocatalysts

It uses artificial neural networks (ANNs) to predict the potential energy. The ANNs are composed of multiple nodes that resemble real brain neurons. The neurons are interconnected and interact with one another [60,62,63]. The nodes can take data as input and perform basic operations on it. A neuron's processing component receives numerous signals. Sometimes, signals are altered at the receiving synapses, and the processing element adds the weighted inputs. The output of the neuron results from a threshold activation function. The advantages of DLS over ML to assess the catalyst behavior are given in Table 3.

The process is repeated if the threshold is crossed, and the signal becomes an input to other neurons. The equation for our model can be expressed as follows:

$$y_i = f(\sum_{i=1}^{n} w_i x_i + b_i) \quad (8)$$

where y_i represents the output of the neuron, x_i represents the input to the neuron, w_i represents the weight of the network, and bi is the bias. Deep learning (DL) is particularly adept at handling complex, unstructured data, such as time-series information and fluid dynamics, where traditional machine learning (ML) techniques often fall short. Its superior accuracy shines in complex tasks, outperforming ML in predicting long-term catalyst degradation, optimizing water management, and analyzing microstructures that involve non-linear, high-dimensional relationships. Additionally, DL models have the unique advantage of continuously learning from extensive and diverse datasets, enhancing their accuracy and efficiency. It is an essential capability for real-world applications like catalyst layer optimization. Their ability to discern intricate non-linear patterns is vital for making precise predictions and optimizations in sophisticated systems such as Proton Exchange Membrane Electrolysis (PEME). In summary, DL emerges as the definitive choice for

analyzing large, complex, and unstructured data, enabling superior performance, accuracy, and adaptability—critical factors for optimizing catalyst layers in advanced technologies.

Table 3. Rationale for choosing DL over ML [64–67].

Aspect	Machine Learning (ML)	Deep Learning (DL)
Key Methods	SVM, Decision Trees, Random Forests, and GA	CNN, RNN, and LSTM
Data Requirements	Works best with structured, smaller datasets	Excels with large, unstructured datasets (images, time series, etc.)
Computational Complexity	Low; can be trained with minimal resources	High; requires specialized hardware (e.g., GPUs)
Efficiency	Fast for simpler, structured tasks	Highly efficient for complex, high-dimensional tasks
Interpretability	High; decisions are easily understood	Often considered a "black box," though compensates with accuracy
Performance of Simple Tasks	Effective for well-defined, straightforward tasks	Less efficient for simple tasks due to the complexity of the models
Performance of Complex Tasks	Struggles with non-linear, high-dimensional relationships	Superior at handling complex, multi-dimensional relationships (e.g., microstructure analysis and fluid dynamics)
Key Use Cases	Fault detection, material optimization, and degradation prediction	Microstructure analysis (CNN), performance forecasting (LSTM), and water management (RNN)
Examples	SVM for fault classification and GA for optimization	CNN for detecting microstructural changes; LSTM for predicting long-term degradation
Outcome	Faster execution and high interpretability for simpler tasks	High accuracy, adaptability to diverse datasets, and the ability to learn complex patterns over time
Challenges	Struggles with unstructured data; limited scalability for complex tasks	Requires large datasets and significant computational power; less transparent decision-making
Supporting Factors	Works well with structured data (e.g., sensors and material composition)	Leverages large and diverse datasets (e.g., imaging and time-series); requires high computational resources
Future Directions	Real-time fault detection and optimization of simpler tasks	Real-time optimization, long-term performance predictions, and reinforcement learning for extreme conditions

3. Materials and Methods

In this section, we report the data collection and methods related to the DFT (Section 3.1) and cell polarization (Section 3.2) and approaches adopted in the deep learning simulations (Section 3.3). The steps associated with the calculation are given in Figure 2.

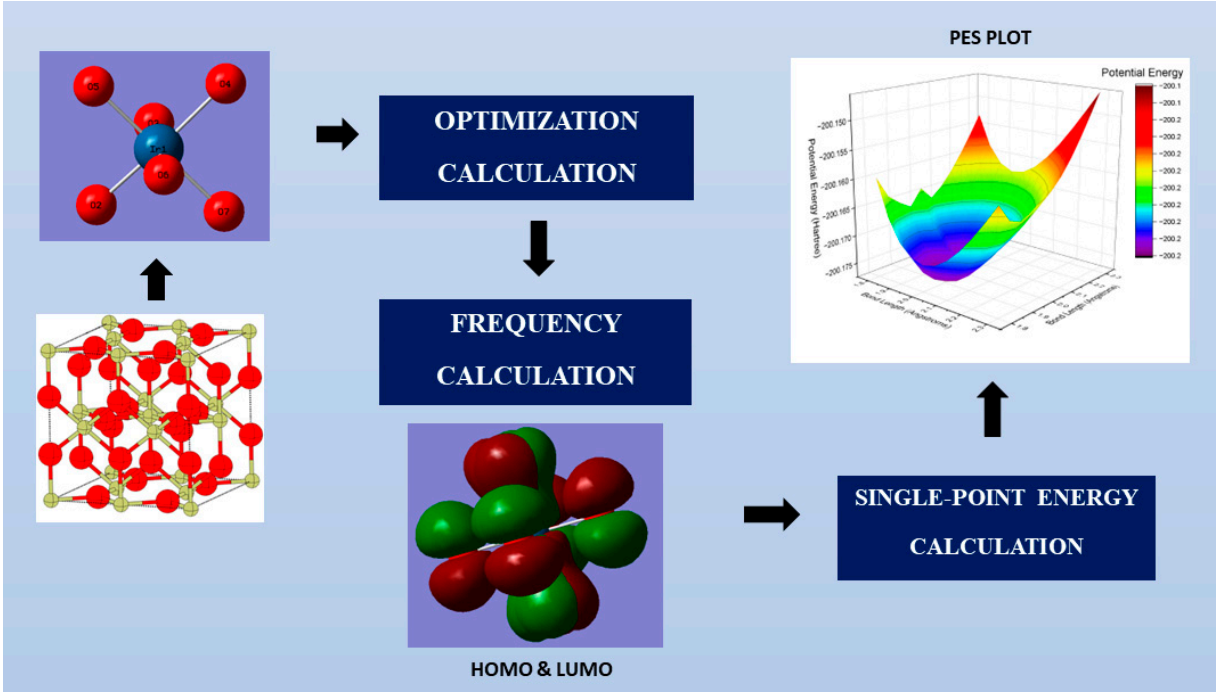

Figure 2. DFT calculation methodology.

3.1. Data Collection and DFT Computation Methods

To optimize our DFT and computational analysis, we selected a single unit cell from the packed structure of Ir-based electrocatalyst, which reduced the system size and computational resource demands. This unit cell accurately represents the crystal structure, preserving its key symmetries and properties. We simplified the packed structure by minimizing the number of atoms, creating a smaller unit cell for the potential energy surface (PES) calculations. This strategic simplification improved analytical efficiency while ensuring the necessary accuracy for this study. We present the packed, unoptimized structure of the catalyst used for the PES calculations here. It is important to note that we have not yet performed energy minimization or relaxation on this structure, which is typically performed to determine the most stable configuration. DFT calculations were conducted using Gaussian 16, with results visualized in GaussView 6. We chose the Perdew–Burke–Ernzerhof (PBE) exchange-correlation functional, recognized for its accuracy in calculating molecular properties like bond lengths and vibrational frequencies [59,68]. The SBKJC-VDZ basis set was employed to evaluate electron density and molecular properties [60], alongside the GENeralized Electronically Contracted Pseudo-atom (GENCEP) basis set for modeling transition metal compounds [62]. For enhanced efficiency, we applied quadratic convergence to speed up computations. We calculated the potential energy surface (PES) through a rigid scan of bond lengths between catalyst metal and oxygen, starting from 1.8 Å in 0.05 Å increments, which aligns with established methodologies [60,62]. The PES calculation involved three steps: optimization, frequency calculations, and single-point energy evaluations, each providing crucial insights into system stability. The optimization aimed to locate the minimum energy configuration of the iridium oxide molecule, using the Self-Consistent Field (SCF) method to iteratively solve Kohn–Sham equations. The quasi-Newton method was employed for gradient-based optimization, effectively enhancing convergence [60]. Frequency calculations confirmed that the optimized structure corresponds to a true minimum energy structure (TMES), based on Hessian matrix analysis to ascertain potential energy surface curvature [63]. Diagonalizing the Hessian provided vibrational frequencies and modes, ensuring stability. Lastly, we constructed the

PES by solving the Schrödinger equation for various geometries using single-point energy calculations. These calculations yield the energy profile critical for understanding catalyst stability with respect to bond length variations, facilitating the mapping of the system's energetics [69].

3.2. Experimental Data Collection

The anode polarization data from an operating electrolyzer cell is needed to assess the OER characteristics of the IrOx. However, a reference electrode configuration is vital to separate the anode polarization data from the overall cell polarization [70]. The steady-state cell and electrode polarization curves were obtained for three different water feed rates and temperatures. The feed rate of 6 mL.min^{-1} was considered for our study. Special attention is paid to the activation region (0.00–0.50 A.cm^{-2}) of the anode polarization curve to compare and contrast the OER characteristics of the IrOx catalyst layer. Computed Tafel slopes were validated against DFT predictions to optimize understanding of the reaction mechanism. Electrochemical stability analyses from DFT were cross-referenced with experimental voltage decay rates.

3.3. Development of DLS Architecture and Data Collection

This section describes the need, rationale, and method used to develop the given molecule's DLS architecture. Machine learning models were used for multivariate analysis to correlate the experimental and computational features, respectively. This approach may provide the key catalyst characteristics that can help to maximize OER efficiency. Predictive models based on both datasets need to be developed to forecast the performance of catalyst layers, driving future catalyst designs. This iterative process of refining catalyst materials through DFT-guided experimentation and machine learning insights optimized catalyst efficiency and stability, positioning this approach as a powerful tool for advancing OER technologies in PEM electrolyzers. However, the data for the DLS model are not available for iridium oxide molecules in any literature. Therefore, to develop and test the DLS architecture, we have collected a dataset from the CHAMP database [71]. It consists of details related to more than 1 lakh molecules of carbon, hydrogen, nitrogen, oxygen, and fluorine. The mean bond length and the number of bonds per atom were also calculated based on the nuclear coordinates using the Euclidean distance. Calculating the potential energy of a molecule using the Gaussian software requires high memory resources and increases computational time. The multiple gradients added in the DFT computation of the IrOx structure require several initial guesses to complete the convergence criteria. It includes the values for (a) maximum force, (b) RMS, (c) maximum displacement, and (d) the RMS displacement. A PES plot obtained for the simplified seven-atomic structure requires 24 h to converge. The complexity of the time steps increases exponentially based on computational requirements. Since IrOx has a complex structure, the convergence took more time according to the number of atoms in the crystals. Therefore, a trade-off between the model's accuracy and sensitivity must be attained based on the trial-and-error approach. However, the literature supports employing the DLS methods that could facilitate faster computation by identifying the key trends on the IrOx in the dataset obtained from the preliminary DFT simulation. Tools such as Gaussian can help match the molecule's point group symmetry with the one in its library. Predicting the potential energy at each atomic coordinate of the iridium oxide molecule requires a DLS algorithm (Figure 3), as the symmetry of the molecule is not in either the Gaussian database or at the point group symmetry assignment. Hence, we manually assigned the symmetry of IrOx based on literature data. It can be avoided using the DLS method, thus simplifying new molecular properties calculations. Therefore, we fed the results of the quantum mechanical

calculations and experimental findings with the IrOx structure as input for the DL model. The model solves non-linearity in the high-dimensional space, and the intricate connections between the potential energy and parameters are computed.

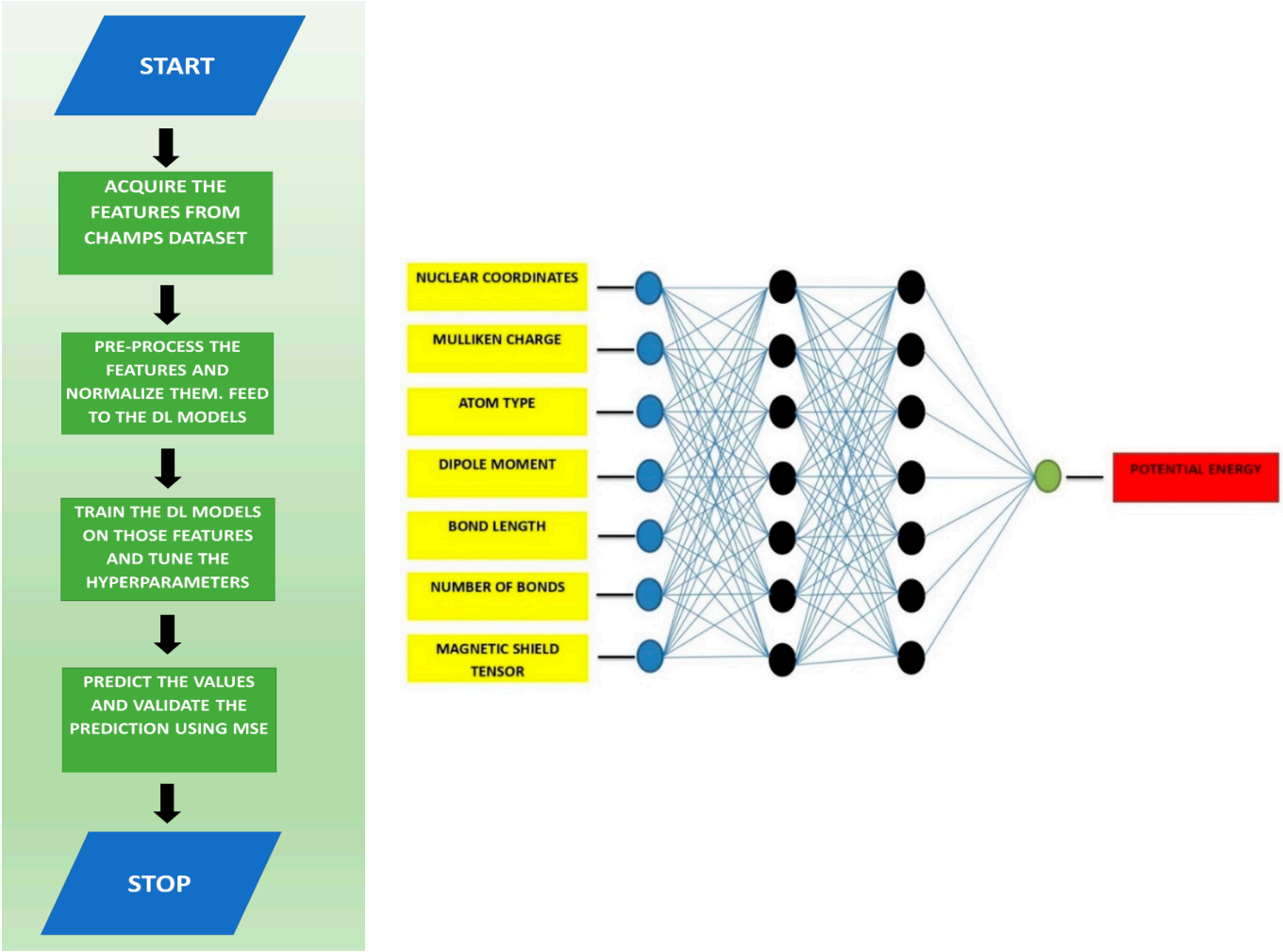

Figure 3. DLS methodology and architecture.

3.4. Feature Importance

XGBoost regressor is used to perform feature importance. It uses a gradient-boosting framework where several decision trees are built [72]. Each tree is trained on a subset of datasets selected randomly from the original dataset. Errors will be estimated iteratively from the first tree in the forest. The next set of trees will correct the errors based on the previous tree data. A new tree is constructed sequentially based on the aforementioned algorithm. The loss function is calculated by the XGBoost algorithm. In order to minimize the loss function, the regressor alters the weights of the individual decision tree during the training of the model. The gradient of the loss function for each data point in the training set is calculated. The mean squared error (MSE) is calculated based on the predicted and actual values using the following formula:

$$MSE = \frac{1}{n}\sum_{i=1}^{n}(Y_i - Y_p)^2 \quad (9)$$

where n stands for the total number of data points, Y_i is the observed value, and Y_p is the predicted value. The overall prediction of the model relies on the predictions obtained for the individual trees.

4. Results and Discussions

4.1. Protocol to Perform the Baseline DFT Analysis to Assess the Molecular Stability of the Electrocatalyst Molecule for PEME Electrolyzer

As the IrO_2 structure was meticulously obtained from COD, initial cell dimensions were provided (Table 4) [73]. This final structure comprises 433 electrons and 11 atoms. For the potential energy surface (PES) calculations, we strategically focused on a single unit cell to enhance computational efficiency. This refinement led to a streamlined structure containing 125 electrons and 7 atoms, enabling more precise analysis. Remarkably, the bond length of the optimized IrO_x structure was determined to be 1.98 Å. Figure 4 captivatingly showcases the packed, unoptimized structure of iridium oxide employed in the PES calculations, highlighting its significance in our study.

Table 4. The IrO_2 crystal data.

Formula	IrO_2
Space Group	P/42
Unit cell dimensions	a = 4.499 Å b = 4.499 Å c = 3.146 Å α = 90 β = 90 γ = 90
Volume	63.678

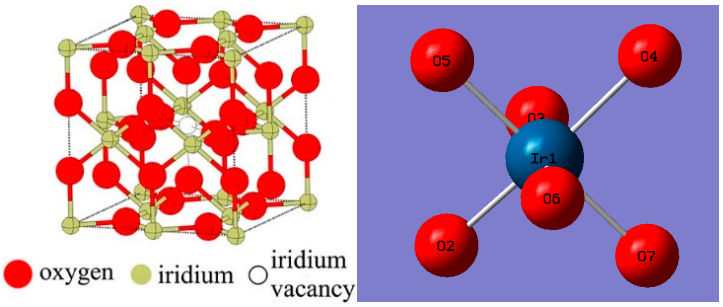

(**a**) (**b**)

Figure 4. (**a**) The packed structure of iridium oxide is shown. (**b**) Unoptimized iridium oxide structure used for PES calculations.

4.2. PES Analysis

In the process of geometrical optimization for IrOx, the algorithm identifies a minimum that closely resembles the original structural configuration. This algorithm is designed to specify both the number of steps required and the incremental distances to be adjusted in order to achieve an optimized structure. The potential energy surface (PES) associated with the geometry of IrOx utilizes the quasi-Newton method, allowing for an accurate estimation of the optimized bond lengths. Following the comprehensive DFT optimization of the molecular structure, the bond lengths (measured in Angstroms) of the optimized structure, which prominently features the central atom iridium, are detailed in the table below. Notably, the average difference in bond lengths calculated between the original and optimized structures reported in Table 5 is indicating significant refinement in the geometry.

Table 5. Comparison between the original (unoptimized) structure and optimized structure.

Atom Number	Bond Length		
	Original Structure (Å)	**Optimized Structure (Å)**	**Literature Review (Å)**
Ir1-O1	2.02	2.015	2.037
Ir1-O2	2.02	1.982	1.917
Ir1-O4	2.02	1.982	1.917
Ir1-O3	1.98	2.015	2.037
Ir2-O3	1.98	1.982	1.917
Details of the optimized structure			
Electronic Energy	−897.67538271487115 Eh		
RMS Gradient Norm	0.0000259925 Hartree/Bohr		
Polarizability (α)	NA		
Diploe Moment	3.412693525 Debye		
Enthalpy (with correction)	−509.11286082 Eh		
Mulliken Charges	Atom Number	Atom	Mulliken Charge (a.u.)
	1	Ir	0.971375
	2	Ir	0.406013
	3	O	−0.304719
	4	O	−0.355709
	5	O	−0.361251
	6	O	−0.355709

4.3. Obtaining the Optimum Bond Length and Bond Angle with HOMO and LUMO Structure for the Same Molecules

The HOMO-LUMO gap is critical in determining the catalytic efficiency of materials such as iridium oxide (IrO_2) in both oxygen evolution reactions (OERs) and oxygen reduction reactions (ORRs), albeit in distinct ways for each process. The energy levels of IrO_2, defined by the highest occupied molecular orbital (HOMO) and the lowest unoccupied molecular orbital (LUMO), are essential for electron transfer during catalysis. For IrO_2, the HOMO-LUMO gap is approximately 0 eV, which reflects its metallic nature and facilitates efficient electron transfer—key for OER. A narrower HOMO-LUMO gap promotes faster electron transfer, reducing overpotentials and enhancing the efficiency of OER by allowing easier excitation of electrons from the HOMO to the LUMO. This feature is fundamental to IrO_2's responsiveness in OER, where its metallic nature creates a highly reactive catalyst under appropriate electrochemical conditions. As highlighted by Nørskov et al. [19], such a minimal gap lowers the activation energy needed for electron transfer, thereby accelerating oxygen evolution. In contrast, for ORR, the HOMO-LUMO gap requires optimization for electron acceptance. A moderate gap in IrO_2 is advantageous for facilitating the multi-electron transfer process involved in ORR, as shown by He et al. [74] and Zhang and Wang [39]. A smaller HOMO-LUMO gap allows for better electron donation, which aids in the reduction of O^{2-} to OH^-. However, if the gap is excessively small, it may lead to the formation of unstable intermediates, disrupting the ORR process. Therefore, to achieve optimal performance, the HOMO-LUMO gap must be carefully tuned for OER, balancing electron donation and acceptance while avoiding unwanted intermediates. A detailed visualization of the IrOx orbitals is illustrated in Figure 5, showcasing the spatial distribution and symmetry of these critical orbitals. During electrochemical reactions, a

dynamic interaction unfolds, i.e., electrophiles at the cathode move to accept electrons, thereby forming bonds with the HOMO. Simultaneously, nucleophiles at the anode donate electrons to the system, creating bonds with the LUMO. This intricate electron transfer process is facilitated by weak van der Waals forces, which play a crucial role in stabilizing these transitional states and promoting effective interactions. Moreover, the energy difference between the HOMO and LUMO, referred to as the HOMO-LUMO gap, serves as a pivotal parameter for deciphering the electronic properties of the Ir-O molecule [5,39,75–82].

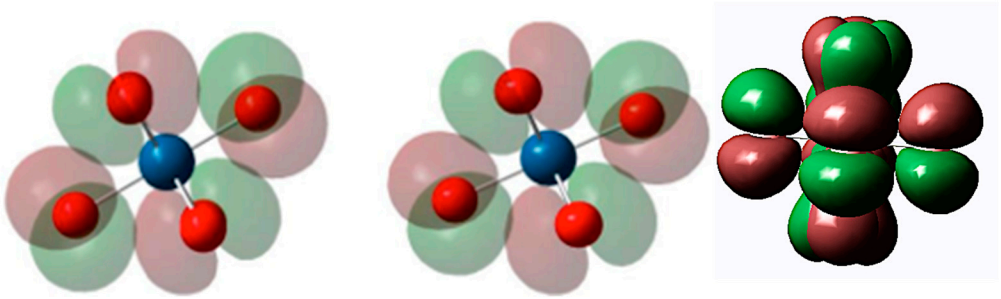

(**a**) (**b**)

Figure 5. The HOMO-LUMO molecular orbitals obtained from the literature [75–77] (**a**,**b**) and those obtained from this study.

Additional molecular properties for IrOx have been calculated and are presented in the table below. Electronegativity is expressed in terms of orbital energies and is calculated using the provided equation. The energy magnitudes of the HOMO and LUMO for the IrOx species were obtained from the potential energy surface (PES) calculations. Furthermore, the ionization energy and electron affinity were estimated using Fukui functions, which have been shown to align closely with predictions based on wavefunction theory. The computed electronegativity (χ) of 0.335 using the formula given below is in good agreement with the literature-reported values.

$$M\chi = \frac{-(E_{HOMO} + E_{LUMO})}{2} \tag{10}$$

Further modifications to the surface structure and oxidation states of IrO_2 can influence the HOMO-LUMO gap and enhance its catalytic performance for redox reactions. Surface vacancies, strain, and alterations in bond angles and bond lengths can shift the electronic structure and subsequent HOMO-LUMO alignment. As noted by Florbela et al. [64], such surface modifications can optimize the adsorption of reactive intermediates like OH^- and O^{2-}, thus improving the activities of both OER and ORR. Mavrikakis et al. [21] emphasized that aligning the HOMO-LUMO levels with the reaction energy profile through structural optimization can reduce energy barriers, thereby enhancing electrocatalytic efficiency. In summary, the HOMO-LUMO gap plays a vital role in electron transfer processes for both OER and ORR, but the optimal gap differs between them. For OER, a narrower gap found (0 eV) in this work facilitates quicker electron transfer and improves oxygen evolution, while for ORR, a moderate gap is necessary for effective electron acceptance without forming unstable intermediates. Optimizing the HOMO-LUMO gap through structural and surface modifications is proven as a factor for enhancing the catalytic activity of materials like IrO_2 in electrochemical reactions. Thus, understanding and controlling the electronic structures of IrO_2 and similar materials is found to be crucial for advancing the fabrication of electrocatalytic layers for electrolyzers.

4.4. Extending DFT to Study the OER Pathway and Develop PES Plots That Can Be Further Used to Identify Reaction Pathways and Reaction Rates and to Understand Reaction Dynamics

To thoroughly illustrate the reaction dynamics of IrOx, we constructed a sophisticated potential energy surface (PES) plot, utilizing an extensive series of optimization and frequency calculations. This comprehensive analysis encompasses the intrinsic reaction coordinate (IRC) pathway, which reveals 121 transition states, as shown in Figure 6. This plot serves as a dynamic portrayal of the potential energy landscape, intricately linked to the coordinates of the iridium atoms and the IrOx molecule, offering profound insights into the energy fluctuations across diverse molecular configurations. This exploration yields crucial insights into the overarching reaction pathway, enabling us to pinpoint potential intermediates and accurately predict the final products of the reaction. The energy barriers separating transition states play an essential role in estimating reaction rates, a factor critical to our understanding of the kinetics governing these complex processes. In Figure 6, the lowest energy point signifies the most stable configuration, while the peaks at higher energy correspond to transition states that reflect the challenges to overcome during the reaction. These energy barriers precisely illustrate the energy demands necessary to navigate the various steps of the reaction, thereby clarifying the mechanisms and reactivity of IrOx under varying conditions. Our in-depth approach to understanding the reaction dynamics of IrOx did not stop at the PES. By incorporating the IRC pathway, we constructed an enriched PES plot that offers an unparalleled view of the intricate energy profile as the reaction progresses from reactants to products. This is compellingly showcased in Figure 6, marrying the potential energy landscape with the coordinates of iridium atoms and the IrOx molecule, thereby delivering a comprehensive understanding of energy transitions across an array of molecular conformations. IRC pathway stands as an indispensable tool in computational chemistry, tracing the reaction path from transition states to both reactants and products, thereby providing invaluable insight into the reaction mechanism. Each identified transition state along the IRC pathway marks a critical juncture in the reaction pathway, enabling a more nuanced and complete description of the energetics compared to the PES alone. By meticulously following this path, we can anticipate potential intermediates that could arise during the reaction, thereby sharpening our focus on the key steps within the reaction mechanism. In our study, the reaction pathway compellingly reveals that the lowest energy point correlates with the most stable configuration, while the highest energy points identify the transition states that must be transcended for the reaction to advance. The energy barriers depicted in the PES plot represent the activation energies essential for each transition state, which are decisively important in determining reaction rates. The IRC analysis significantly enhances our grasp of reaction kinetics, allowing for precise estimation of these energy barriers. Our findings underscore that the energy barriers are notably low, aligning seamlessly with the metallic characteristics of IrO_2. This facilitates rapid electron transfer, positioning IrO_2 as an exceptionally efficient catalyst for processes such as oxygen evolution. In comparing our results to established literature, the IRC pathway analysis resonates powerfully with the discoveries of He et al. [74] and Zhang et al. [18]. Both studies confirm that IrOx, particularly IrO_2, showcases impressively low energy barriers during the oxygen evolution reaction (OER), reinforcing its metallic behavior. Furthermore, the energy profile we obtained robustly supports these observations, demonstrating that the transition states are consistent with the low overpotentials required for efficient OER catalysis. The analysis is also in full agreement with the groundbreaking work of Nørskov et al. [19], which illustrated the significance of reducing energy barriers for effective OER performance in oxide catalysts like IrOx. Our findings affirm that the relatively flat PES and low activation energies are indeed critical factors contributing to the superior catalytic efficiency of IrO_2. Moreover, research by Duthie et al. [19–74,83,84]

illustrates the substantial influence of the oxidation state of IrO_2 on modulating energy barriers during OER. Our IRC pathway analysis further validates this, indicating that changes in oxidation state considerably influence the stability of transition states and reaction intermediates, thereby directly enhancing OER efficiency. In conclusion, our integration of the IRC pathway into the PES analysis offers a transformative perspective on the reaction dynamics of IrOx. The detailed energy landscape we uncovered illuminates the favorable catalytic properties of IrO_2 with striking clarity. This comparison with existing literature not only validates our computational methodology but also underscores the coherence of our findings with experimentally observed reaction mechanisms, thus reinforcing the compelling nature of our research.

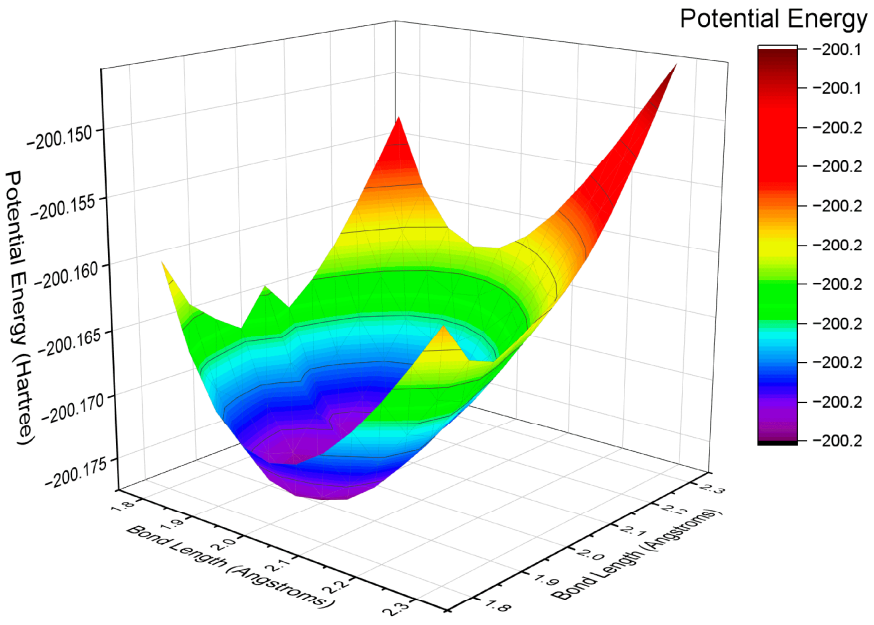

Figure 6. PES plot.

4.5. Correlating the OER Data Obtained from the PEM Electrolyzer with Reference Electrode Cell to DFT Data Obtained from the Simulation

Steady-state oxygen evolution reaction (OER) polarization curves were meticulously replotted based on the work of Elyse et al. [70] (Figure 7) to provide a comprehensive overview of the anode performance. Figure 7 presents the polarization curves for the anode OER, depicted in red, alongside the cathode hydrogen evolution reaction (HER) in blue, and the overall cell performance illustrated in black. These curves were generated under three different feed rates and temperatures, allowing for a comparative analysis. To elucidate the reaction mechanism behind the OER, we closely examined the activation region of each OER curve, specifically within the range of 0.00 to 0.50 A·cm^{-2}. The reference electrode setup utilized in the experiments provides valuable anode polarization data that are essential for assessing the rate-determining step and overall mechanism of the reaction. Notably, the Tafel slopes calculated from the activation-controlled regions exhibited a twofold increase when the temperature was raised from 40 °C to 80 °C. At 80 °C, the observed exchange current density was measured at 8.6×10^{-1} A·cm^{-2}, with a Tafel slope of −100.7 mV/decade. This low exchange current density for the anode indicates that the kinetics of the OER are significantly slower compared to those of the cathode. The reaction scheme governing the OER can be succinctly represented through Equations (11)–(13), which detail the fundamental steps involved in the process. This comprehensive analysis

contributes to a deeper understanding of the mechanisms at play in the OER and the implications for overall cell performance.

$$\mathrm{MOx} + H_2O \rightleftarrows \mathrm{M} - OH_{ads} + e^- + H^+ \quad (11)$$

$$\mathrm{M}- OH_{ads} \rightleftarrows \mathrm{M} - O_{ads} + e^- + H^+ \quad (12)$$

$$2(\mathrm{M} - O_{ads}) \rightleftarrows O_2 + 2\mathrm{M} \quad (13)$$

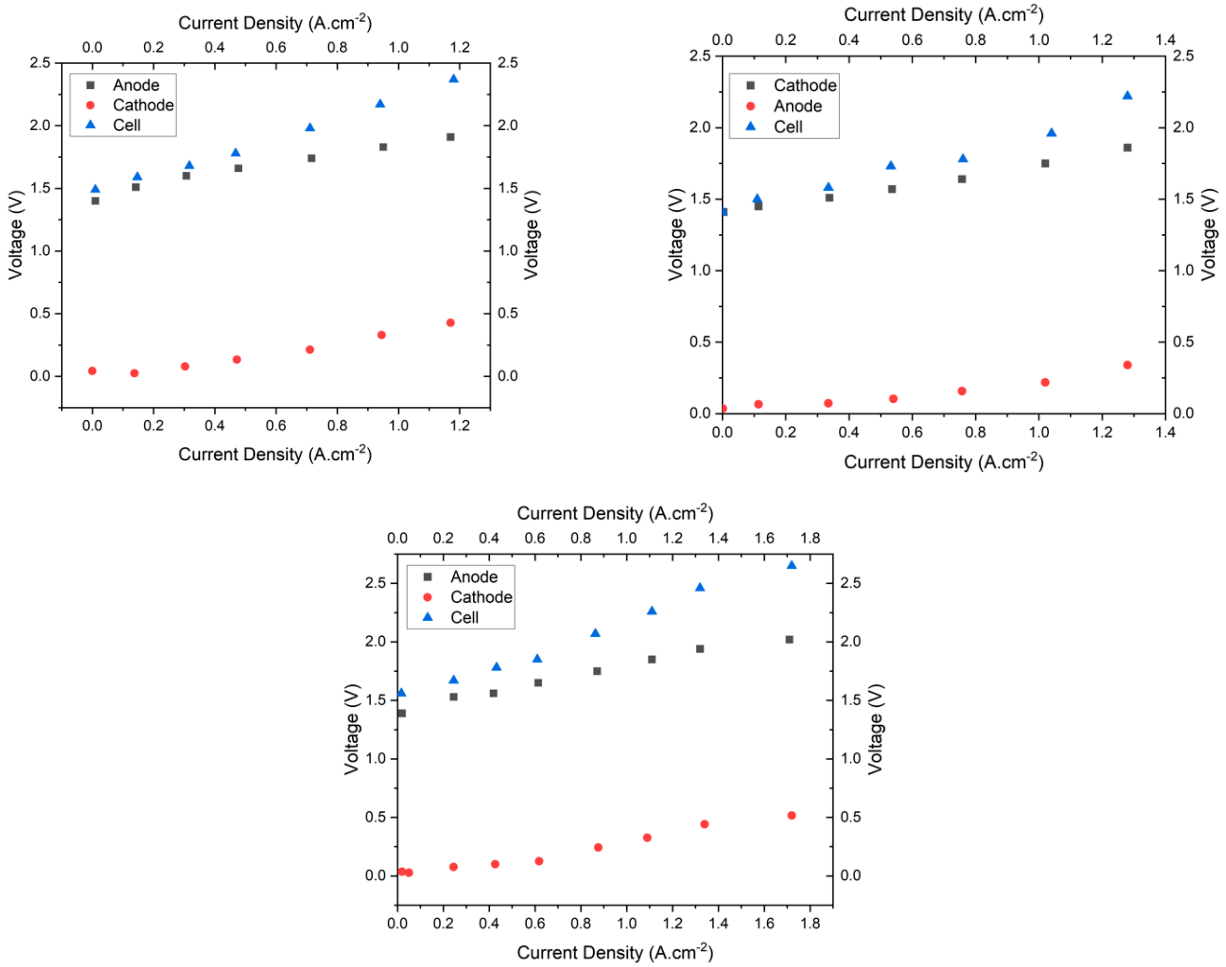

Figure 7. Anode, cathode, and cell polarization curve at 40 °C, 60 °C, and 80 °C.

The Tafel slope and exchange current density data provide compelling evidence that the oxygen evolution reaction (OER) occurs primarily through the electrochemical oxide pathway, as detailed in Equations (11)–(13). This pathway culminates in the generation of oxygen. In the pivotal charge transfer step, represented in Equation (13), a nuanced interaction takes place on the catalyst surface, denoted as M. In this step, an electron, a proton, and an adsorbed hydronium ion coalesce, a process that necessitates the availability of two catalyst sites to facilitate both the adsorption of oxygen and its eventual production. The electronic structure of IrOx is fundamental to its electrochromic properties and plays a crucial role in determining its exchange current density, a key indicator of its catalytic efficacy. A comprehensive evaluation of the OER, alongside a detailed analysis of the geometric structure of IrOx and its electronic configuration, establishes a substantive connection between the electrocatalytic activity and the polarization behavior of the electrode. Moreover, the optimized structure of the catalyst layer significantly enhances the binding strength during the OER phase. This optimization results in the generation of precise

d-spacing, which is instrumental in improving charge transfer at the electrode–electrolyte interface. Such enhancements facilitate more effective electrochemical reactions by allowing for better electron and ion transport within the system. This integrated approach not only illustrates the critical relationship between structural attributes and electronic properties but also underscores the potential of IrOx as a high-performing catalyst for the OER.

4.6. Developing a Deep Learning Model to Assess the Predictive Maintenance for the Support Molecules of the Electrocatalyst

The composition of IrOx/ionomer/carbon catalyst layers includes iridium oxide, ionomer binders, and carbon supports, all of which are critical for efficient charge transfer. Artificial intelligence (AI), particularly machine learning (ML), plays a vital role in optimizing this material composition to enhance catalytic performance while reducing costs. Moreover, deep learning (DL) models analyze changes to identify and design innovative materials. The thickness of these catalyst layers also significantly impacts conductivity and the availability of active sites; if the layer is too thick, efficiency can be compromised, while a layer that is too thin may not provide sufficient active sites for optimal performance. AI techniques are deployed to fine-tune layer thickness based on operational conditions, achieving an ideal balance between efficiency and durability, with ML addressing simpler thickness modeling and DL being utilized for more complex structural analyses. The protocol adopted to perform the DL simulation is given in Figure 8. Features in machine learning are essential components of a dataset. In this research, descriptors such as dipole moment, Mulliken charge, and nuclear coordinate are classified as feature datasets. The identification and assignment of weights to these features are contingent upon the Deep Learning Surrogate (DLS) model employed. The primary analysis of feature significance is vital for optimizing the model training process, as it contributes to reducing training time, minimizing redundancy, and preventing overfitting. For instance, as depicted in Figure 8, the dipole moment is identified as a significant feature, assigned a weight of 0.19. Conversely, features related to atomic properties and structural characteristics exhibit less weight compared to the dipole moment. It is important to note that the weighting of each feature may vary depending on the specific dataset in use. By leveraging the insights provided in Figure 8, one can strategically select features for training the DLS model based on their assigned weights. This approach ensures the prioritization of the most relevant features, ultimately enhancing the efficiency and effectiveness of the modeling process.

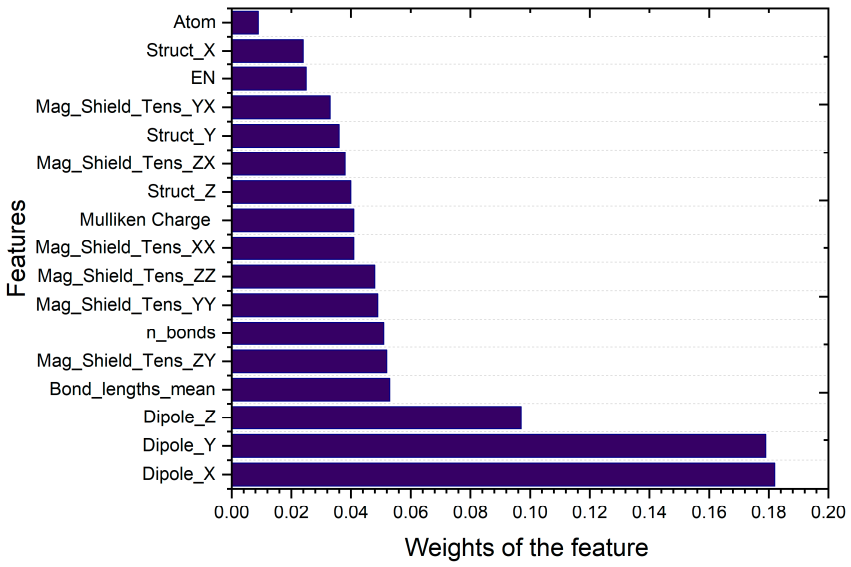

Figure 8. Feature importance plot.

4.6.1. t-SNE Plots

A t-Distributed Stochastic Neighbor Embedding (t-SNE) plot is presented to visualize the CHAMP datasets. This plot successfully transforms a higher-dimensional dataset into a lower-dimensional representation by executing pairwise similarity (PS) calculations. The PS method proficiently organizes and maps data points in the high-dimensional space while maintaining the inherent relationships and similarities in the lower-dimensional space [72–74,84]. Figure 9 distinctly illustrates the mapping and organization of potential energy in relation to its associated features. Each atom, including carbon, hydrogen, oxygen, fluorine, and nitrogen, is clearly identified without any overlapping or clustering. Consequently, the algorithms employed in the deep learning (DL) model can effectively utilize the trends established in this study to predict or assess the properties of unknown molecules. This capability significantly enhances the model's predictive power across various applications.

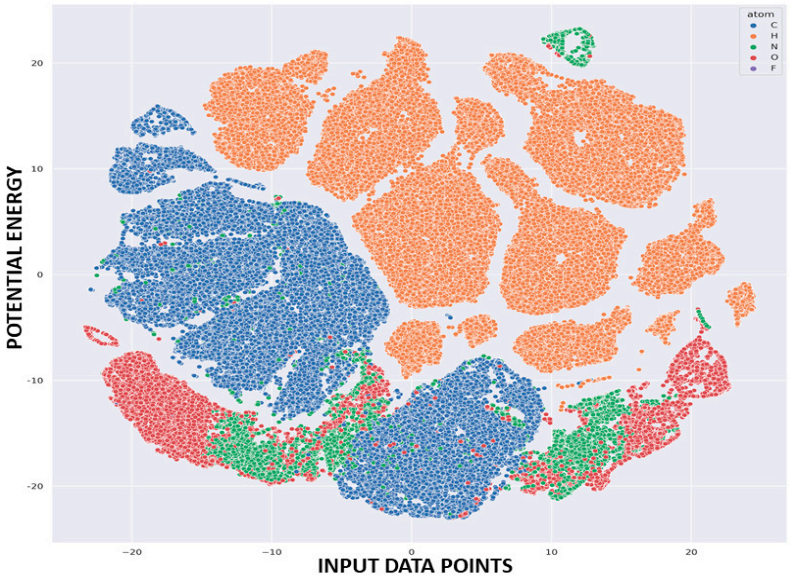

Figure 9. t-SNE plot for our dataset.

4.6.2. Comparison of ANN-Based DLS Models

To comprehensively evaluate the architecture of the Deep Learning Surrogate (DLS), we undertook an extensive performance analysis of three distinct artificial neural network (ANN)-based DLS models (Table 6), each characterized by different structural configurations comprising 10, 12, and 14 blocks. Each block is designed to include four essential layers: a dense layer, a batch normalization layer, a LeakyReLU activation layer, and a dropout layer, each serving a specific function within the architecture. The dense layer is a crucial element of the ANN structure, facilitating a direct connection between the input data and the output neurons. This layer effectively transforms the input information into meaningful predictions. The batch normalization layer improves the stability and performance of the neural network by standardizing the activations of each layer, thereby accelerating training and contributing to more robust model convergence. This standardization minimizes internal covariate shifts and ensures that the training process progresses smoothly [78–82].

Table 6. Comparison between the three models.

Number of Blocks	10	12	14
Number of Layers	40	49	56
Optimizer	AdaMax	AdaMax	AdaMax
Learning Rate	0.0099	0.0099	0.0099
Epochs	500	500	500
Training Accuracy (MSE)	0.56	0.46	0.45
Training Time	~125 min	~135 min	~150 min

The LeakyReLU activation layer is implemented to enhance the overall efficiency of the ANN. By allowing a small, non-zero gradient when the unit is not active, it helps mitigate the problem of vanishing gradients and supports better learning. In addition, the dropout layer plays a significant role in combating overfitting by randomly setting a fraction of input units to zero during training, thereby encouraging the model to learn more generalizable features rather than overly specific ones. Table 6 provides a comparative analysis of the three models, revealing that while the 14-block model achieves a lower mean squared error (MSE) than the 12-block model, it also demands greater computational resources, resulting in longer processing times. This observation underscores the importance of balancing accuracy with computational efficiency. In this light, the 12-block model emerges as the optimal choice among the three configurations. Figure 10 illustrates this model's performance, which effectively maintains a high level of accuracy while achieving a remarkable 12-fold reduction in computation time compared to traditional Density Functional Theory (DFT) calculations. This significant computational advantage highlights the practical applicability of the 12-block model for rapid predictions in fields requiring extensive computational resources. Catalyst microstructure characteristics, such as porosity and morphology, play a pivotal role in influencing surface area and electrolysis efficiency. Cutting-edge AI models, particularly deep learning (DL) approaches utilizing convolutional neural networks (CNNs), are revolutionizing the analysis of scanning electron microscope (SEM) images by accurately detecting microstructural changes and significantly enhancing catalyst properties. As the interactions between electrolytes and catalysts are critical for optimizing reaction rates and ensuring stability, and AI-driven simulations are drastically improving electronic and ionic conduction, thereby boosting overall efficiency. Furthermore, the degradation of catalysts due to catalyst/support poisoning, support corrosion, or excessive use of the electrode—electrolyte poses a substantial challenge to model. However, with the predictive capabilities of DL models, we can anticipate these issues, enabling timely maintenance and extending the life of catalysts or support. Effective catalyst management is essential to prevent dissolution or degradation within the catalyst layer. Innovative AI solutions are needed to optimize catalyst–support–ionomer distribution using DL for fluid dynamics simulations and recurrent neural networks (RNNs) for robust time-series analysis. Ensuring uniformity in the catalyst layer is crucial for reliable and consistent performance. Although AI techniques, including ML and Genetic Algorithms (GAs), provide powerful enhancements to deposition methods like sputtering, leading to reduced costs and improved electrolysis efficiency, DL shows promise to improve the accuracy of predictive maintenance. In conclusion, DL is exceptionally effective for structured tasks like fault detection, catalyst layer material efficiency optimization, and degradation forecasting, delivering rapid, actionable insights even with smaller datasets. Meanwhile, DL excels in managing complex, unstructured data, such as images and long-term performance predictions. Together, ML and DL are transforming the optimization of catalyst layers in Proton Exchange Membrane Electrolysis (PEME) systems, significantly enhancing efficiency, performance, and longevity while minimizing costs and downtime.

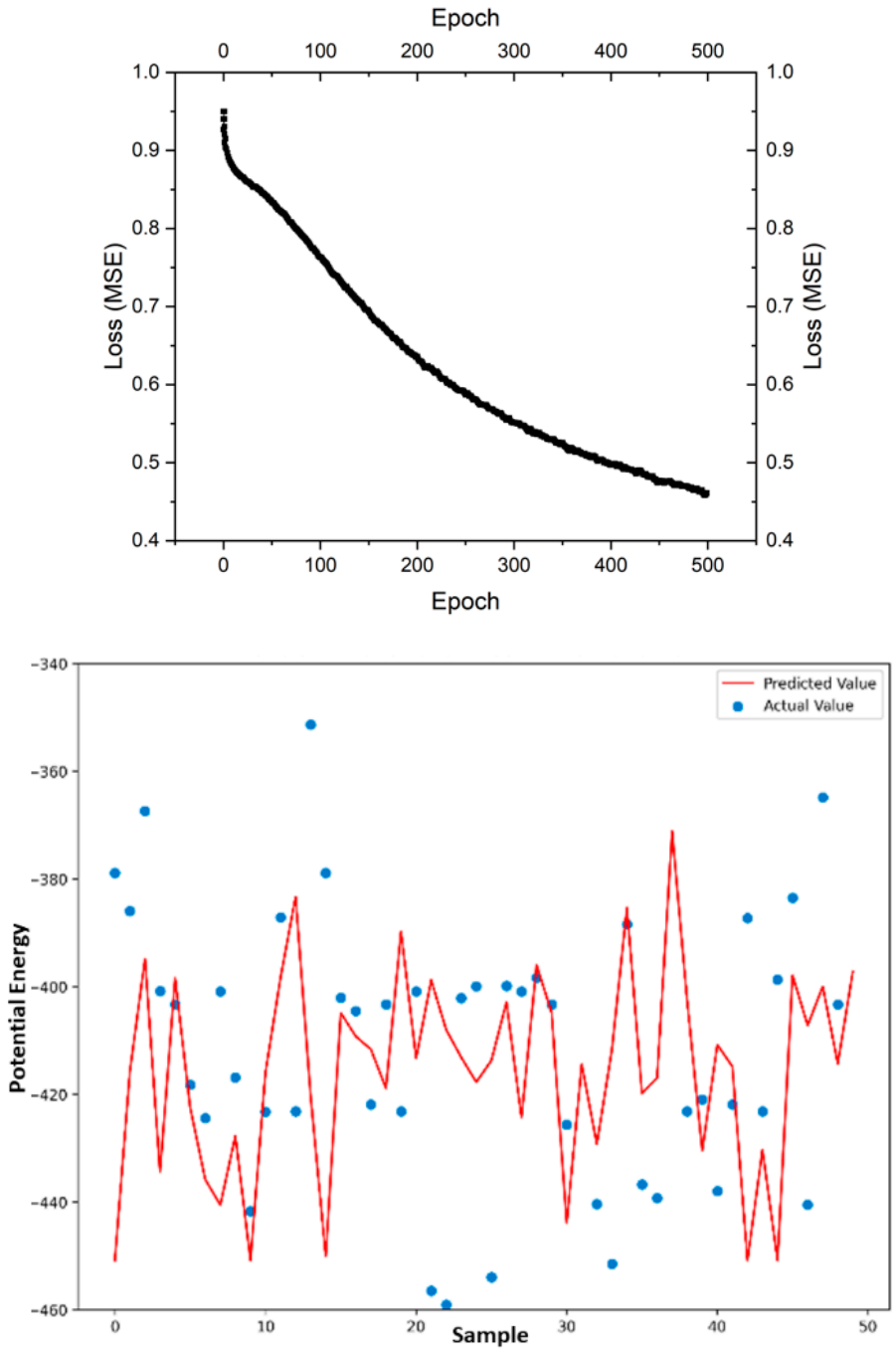

Figure 10. The graph of epoch vs. loss and parity plot for the 12-block model.

Figure 10 shows how the loss changes against the epoch and the parity plot for 12-block models. An increase in epochs shows a negative exponentially decaying trend in loss. Since no change in loss appeared beyond 500, computation or model training can be stopped at the epoch.

4.6.3. Applicability of the DFT-DLS Framework

The proposed framework aims to achieve the following:

- Provide artificial intelligence-based experimental guidance and concept verification for electrocatalysts and support materials.
- Simplify the DFT-DLS concepts and evaluate the chemical and electrochemical properties of the catalyst and support material used in the electrochemical cells.
- Determine the activity and selectivity of the electrocatalyst.

- Benchmark the calculated values to discover new catalysts.
- Develop high-activity, industrial-scale catalysts.
- Develop an AI-based strategy to address catalyst failure modes and mechanisms.
- Assess the temporal variations in the catalyst/support materials that will uncover the surface chemistry of the new materials.

Future study of the framework: The model can be improved further to assess the defects in the materials and learn how the catalyst interacts with different support materials. Presently, we are carrying out a computation process to optimize the active sites based on the catalyst/support surface structures. Furthermore, enhancing the framework will help to set metrics to couple the DFT-DLS theory with experiments and expedite new surface science breakthrough experiments.

5. Conclusions

Advanced technologies are paramount for driving sustainable energy conversion and consumption, essential in the fight against climate change. Achieving sustainability relies heavily on the development of efficient energy storage systems that effectively capture excess energy from renewable sources. One of the most promising methods for storage is in the form of hydrogen, generated through water electrolysis, along with the enhancement of fuel cell performance for large-scale applications. Catalyst efficiency is a critical element in optimizing these energy systems. Ab initio methods, particularly Density Functional Theory (DFT), have demonstrated exceptional effectiveness in modeling new catalytic materials, evaluating their performance, and predicting their reliability for future applications. However, these techniques can be computationally demanding, requiring millions of energy gradient calculations to achieve high-accuracy results, which often limits practitioners to single initial calculations, such as one-particle energy collisions. This study confidently investigates the potential of leveraging Deep Learning Simulations (DLS) to calculate molecular potential energy—a key factor in material feasibility testing—in a significantly less computationally intensive manner. By embracing this approach, we can efficiently test new molecules and dopants specifically for catalysts like IrOx and PtOx. To elevate the model's robustness and accuracy even further, it is imperative to integrate additional predictive features, such as distance matrices, molecular geometry, intermolecular forces, and molecular size. Continued optimization of DLS parameters will be crucial for enhancing predictive capabilities. This study positions itself at the forefront of innovation in sustainable energy technologies, promising to streamline the development of efficient catalysts and energy systems.

Author Contributions: Software S.R.D.; validation, S.R.D., M.W.F. and J.Z.; formal analysis, S.R.D.; re-investigation, D.T., J.T. and S.R.D.; resources, B.A.P.; data curating, S.R.D., T.S. and J.Z.; writing—original draft preparation, S.R.D.; writing—review and editing, S.R.D. and M.W.F.; visualization, S.R.D. and J.T.; supervision, B.A.P. and S.R.D. All authors have read and agreed to the published version of the manuscript.

Funding: This research received no external funding.

Data Availability Statement: The data used for the artificial neural network model are available at: (accessed on 3 February 2024) https://www.kaggle.com/datasets/linhlpv/champsscalarold.

Acknowledgments: The authors would like to thank fuel cell research group members at the Queens University for their continuous support of experimental studies. The proofreading support provided by affiliated universities via the AI-powered Grammarly is duly acknowledged.

Conflicts of Interest: The authors report no conflicts of interest.

References

1. Forsberg, C.W. Future hydrogen markets for large-scale hydrogen production systems. *Int. J. Hydrogen Energy* **2007**, *32*, 431–439. [CrossRef]
2. Jiao, Y.; Zheng, Y.; Jaroniec, M.; Qiao, S.Z. Design of electrocatalysts for oxygen-and hydrogen-involving energy conversion reactions. *Chem. Soc. Rev.* **2015**, *44*, 2060–2086. [CrossRef]
3. Sheng, W.; Gasteiger, H.A.; Shao-Horn, Y. Hydrogen oxidation and evolution reaction kinetics on platinum: Acid vs alkaline electrolytes. *J. Electrochem. Soc.* **2010**, *157*, B1529. [CrossRef]
4. Borup, R.; Krause, T.; Brouwer, J. Hydrogen is essential for industry and transportation decarbonization. *Electrochem. Soc. Interface* **2021**, *30*, 79. [CrossRef]
5. Zhang, X.; Zhang, Z.; Li, H.; Gao, R.; Xiao, M.; Zhu, J.; Feng, M.; Chen, Z. Insight into heterogeneous electrocatalyst design understanding for the reduction of carbon dioxide. *Adv. Energy Mater.* **2022**, *12*, 2201461. [CrossRef]
6. Feng, Q.; Wang, Q.; Zhang, Z.; Xiong, Y.; Li, H.; Yao, Y.; Yuan, X.-Z.; Williams, M.C.; Gu, M.; Chen, H.; et al. Highly active and stable ruthenate pyrochlore for enhanced oxygen evolution reaction in acidic medium electrolysis. *Appl. Catal. B Environ.* **2019**, *244*, 494–501. [CrossRef]
7. Spoeri, C.; Kwan, J.T.H.; Bonakdarpour, A.; Wilkinson, D.P.; Strasser, P. The stability challenges of oxygen evolving catalysts: Towards a common fundamental understanding and mitigation of catalyst degradation. *Angew. Chem. Int. Ed.* **2017**, *56*, 5994–6021. [CrossRef] [PubMed]
8. Jäger, M.O.J.; Morooka, E.V.; Canova, F.F.; Himanen, L.; Foster, A.S. Machine learning hydrogen adsorption on nanoclusters through structural descriptors. *npj Comput. Mater.* **2018**, *4*, 37. [CrossRef]
9. Hammes-Schiffer, S.; Galli, G. Integration of theory and experiment in the modelling of heterogeneous electrocatalysis. *Nat. Energy* **2021**, *6*, 700–705. [CrossRef]
10. Hubert, M.A.; Patel, A.M.; Gallo, A.; Liu, Y.; Valle, E.; Ben-Naim, M.; Sanchez, J.; Sokaras, D.; Sinclair, R.; Nørskov, J.K.; et al. Acidic oxygen evolution reaction activity-stability relationships in Ru-based pyrochlores. *ACS Catal.* **2020**, *10*, 12182–12196. [CrossRef]
11. Duca, M.; Koper, M.T.M. Powering denitrification: The perspectives of electrocatalytic nitrate reduction. *Energy Environ. Sci.* **2012**, *5*, 9726–9742. [CrossRef]
12. McArdle, S.; Endo, S.; Aspuru-Guzik, A.; Benjamin, S.C.; Yuan, X. Quantum computational chemistry. *Rev. Mod. Phys.* **2020**, *92*, 015003. [CrossRef]
13. Siegbahn, P.; Liu, B. An accurate three-dimensional potential energy surface for H_2. *J. Chem. Phys.* **1978**, *68*, 2457–2465. [CrossRef]
14. Fu, C.; Liu, C.; Li, T.; Zhang, X.; Wang, F.; Yang, J.; Jiang, Y.; Cui, P.; Li, H. DFT calculations: A powerful tool for better understanding of electrocatalytic oxygen reduction reactions on Pt-based metallic catalysts. *Comput. Mater. Sci.* **2019**, *170*, 109202. [CrossRef]
15. Sanchez-Castillo, A.; Ruiz, P.; Prez-Ramrez, J.; Corma, A. DFT study on the influence of preparation methods on the catalytic activity of gold nanoparticles. *J. Catal.* **2015**, *328*, 81–92.
16. Mavrikakis, M.; Hammer, B.; Norskov, J.K. Catalytic activity of metal surfaces: Density functional theory studies of surface reactivity. *J. Chem. Phys.* **2001**, *115*, 17–28.
17. Prez-Ramrez, J.; van Santen, R.A.; Corma, A. Theoretical studies on the role of surface defects and preparation methods in the catalytic performance of metal oxides. *Chem. Soc. Rev.* **2008**, *37*, 724–740.
18. Zhang, J.; Liu, P.; Wang, H.; Norskov, J.K. The role of electronic structure in the catalytic performance of metal alloys: A DFT study of platinum-based catalysts. *Nat. Commun.* **2016**, *7*, 10661.
19. N0rskov, J.K.; Bligaard, T.; Rossmeisl, J.; Christensen, C.H. Origin of the overpotential for oxygen reduction at a fuel-cell cathode. *Nature* **2009**, *449*, 1033–1036. [CrossRef] [PubMed]
20. Vojvodic, A.; Chorkendorff, I.; Norskov, J.K. From first principles to catalyst design: A theoretical perspective on CO_2 hydrogenation. *Nat. Mater.* **2014**, *13*, 210–215.
21. Mavrikakis, M.; Rossmeisl, J. Design principles for catalytic CO oxidation: Insights from density functional theory. *J. Phys. Chem. B* **2005**, *109*, 8403–8410.
22. Lu, Q.; Hutchings, G.S.; Yu, W.; Zhou, Y.; Forest, R.V.; Tao, R.; Rosen, J.; Yonemoto, B.T.; Cao, Z.; Zheng, H.; et al. Highly porous non-precious bimetallic electrocatalysts for efficient hydrogen evolution. *Nat. Commun.* **2015**, *6*, 6567. [CrossRef] [PubMed]
23. Jiao, F.; Zheng, Y.; Chen, W. Design of efficient electrocatalysts for the hydrogen evolution reaction: Insights from density functional theory. *Nat. Mater.* **2015**, *17*, 298–304.
24. Huang, J.; Wang, L.; Zhang, Y. 3D electrode design for high-performance electrocatalysis. *Nat. Commun.* **2017**, *8*, 10041.
25. Zhou, Y.; Wang, X.; Liu, X. Three-dimensional porous structures as advanced electrocatalysts for water splitting. *Nat. Commun.* **2020**, *11*, 4257.
26. Li, Y.; Li, H.; Liu, L. 3D catalyst design for hydrogen evolution reaction: Simulating reaction kinetics and overpotential on structured electrodes. *Nat. Commun.* **2018**, *9*, 2040.

27. Tang, C.; Zhang, Z.; Xu, Y. Designing 3D nanostructures for electrocatalysis: Insights into water splitting reactions. *Adv. Energy Mater.* **2021**, *11*, 2003519.
28. Barbosa, A.; Dijkstra, J.; Corma, A. Challenges and strategies for simplifying computationally expensive high-level methods in catalytic simulations. *Nat. Commun.* **2020**, *11*, 3777.
29. Henkelman, G.; Uberuaga, B.P.; Jonsson, H. A fast and accurate algorithm for Bader analysis of charge transfer in solids. *J. Chem. Phys.* **2000**, *113*, 8664–8672.
30. Jain, A.; Agrawal, A.; Choudhary, A. Commentary: The materials project: A materials genome approach to accelerating materials innovation. *AIP Adv.* **2011**, *1*, 011200. [CrossRef]
31. Jones, R.O.; Gunnarsson, O. The density functional formalism, its applications and implications. *Rev. Mod. Phys.* **1989**, *61*, 689–746. [CrossRef]
32. Ramakrishnan, R.; Rupp, M.; Liu, J. Quantum chemistry structures and properties of 134k organic molecules. *Sci. Data* **2015**, *2*, 150009.
33. Kresse, G.; Furthmüller, J. Efficient iterative schemes for ab initio total-energy calculations using a plane-wave basis set. *Phys. Rev. B* **1996**, *54*, 11169–11186. [CrossRef] [PubMed]
34. Stewart, J.J.P. Optimization of parameters for semiempirical methods. I. Method. *J. Comput. Chem.* **2007**, *28*, 2363–2374. [CrossRef]
35. GàöàÇrling, A.; Dreizler, R.M. Density functional theory: From the homogeneous electron gas to molecular systems. *Rev. Mod. Phys.* **1994**, *66*, 114–152.
36. Liu, Y.; Wang, D.; Zhang, S. Electrocatalysis of oxygen evolution and hydrogen evolution: Fundamental insights from computational modeling. *Nat. Mater.* **2016**, *15*, 435–450. [CrossRef]
37. Ke, S.; Rui, C.; Chen, G.; Ma, X. Mini review on electrocatalyst design for seawater splitting: Recent progress and perspectives. *Energy Fuels* **2021**, *35*, 12948–12956. [CrossRef]
38. Ranjan, V.; Puebla-Hellmann, G.; Jung, M.; Hasler, T.; Nunnenkamp, A.; Muoth, M.; Hierold, C.; Wallraff, A.; Schönenberger, C. Understanding atomic interactions in mixed oxide catalysts: Insights from computational chemistry. *Nat. Commun.* **2015**, *6*, 7165. [CrossRef] [PubMed]
39. Wu, S.; Zheng, S.; Zhang, W.; Zhang, M.; Li, S.; Pan, F. Machine-learning prediction of facet-dependent CO coverage on Cu electrocatalysts. *ChemRxiv* **2024**. [CrossRef]
40. Jha, A.; Mavrikakis, M. Machine learning for electrocatalysis: Recent advances, challenges, and opportunities. *Nat. Commun.* **2020**, *11*, 1–12.
41. Li, Z.; Wang, S.; Chin, W.S.; Achenie, L.E.; Xin, H. High-throughput screening of bimetallic catalysts enabled by machine learning. *J. Mater. Chem. A* **2017**, *5*, 24131–24138. [CrossRef]
42. Chen, S.; Zhao, Z.; Gong, Y.; Tang, M.; Xie, L.; Lu, X.; Liu, X.; Zeng, D.; Zhang, L.; Zhang, Q.; et al. Machine learning-based discovery of nickel-based alloys for efficient electrocatalysis. *Nat. Mater.* **2021**, *20*, 694–701. [CrossRef]
43. Yang, H.; Xu, Y.; Li, Y.; Du, X.; Zhang, L.; Wu, Z.; Yang, J.; Yang, Z.; Wang, X.; Wang, H.; et al. Accelerating electrocatalyst discovery with deep learning for enhanced oxygen reduction and evolution. *Nat. Commun.* **2021**, *12*, 4161. [CrossRef]
44. Chen, W.; Li, Y.; Zhang, G.; Wang, H.; Yang, H.; Liang, Y.; Xu, Z.; Liu, H.; Zheng, Y. Accelerating electrocatalyst discovery with deep learning and density functional theory: The case of CO_2 activity reduction. *Nat. Commun.* **2021**, *12*, 1–9. [CrossRef]
45. Liu, Z.; Wang, H.; Xie, L.; Zhang, L.; Gong, Y.; Sun, J.; Han, Y.; Wang, H.; Li, J.; Dai, H. Synergizing deep learning and density functional theory for efficient screening of electrocatalysts. *Nat. Mater.* **2020**, *19*, 592–599. [CrossRef]
46. Li, Y.; Wang, H.; Li, J.; Wang, J.; Zhang, L.; Li, L.; Xie, L.; Chen, W. Graph neural networks for predicting catalytic properties in electrocatalysis. *Nat. Mater.* **2020**, *19*, 801–809. [CrossRef]
47. Umer, M.; Umer, S.; Zafari, M.; Ha, M.; Anand, R.; Hajibabaei, A.; Abbas, A.; Lee, G.; Kim, K.S. Machine learning assisted high-throughput screening of transition metal single atom based superb hydrogen evolution electrocatalysts. *J. Mater. Chem. A* **2022**, *10*, 6679–6689. [CrossRef]
48. Jiang, C.; He, H.; Guo, H.; Zhang, X.; Han, Q.; Weng, Y.; Fu, X.; Zhu, Y.; Yan, N.; Tu, X.; et al. Transfer learning guided discovery of efficient perovskite oxide for alkaline water oxidation. *Nat. Commun.* **2024**, *15*, 6301. [CrossRef] [PubMed]
49. Shan, J.; Li, X.; Wang, H. Quantitative structure-activity relationship models integrated with machine learning for electrocatalyst screening. *Nat. Commun.* **2021**, *12*, 4236. [CrossRef]
50. Hohenberg, P.; Kohn, W. Inhomogeneous electron gas. *Phys. Rev.* **1964**, *136*, B864–B871. [CrossRef]
51. Kohn, W.; Sham, L.J. Self-consistent equations including exchange and correlation effects. *Phys. Rev.* **1965**, *140*, A1133–A1138. [CrossRef]
52. Schrödinger, E. An undulatory theory of the mechanics of atoms and molecules. *Phys. Rev.* **1926**, *28*, 1049–1070. [CrossRef]
53. Soper, A.K. The application of quantum mechanics to condensed matter. *Nat. Phys.* **2005**, *1*, 7–13. [CrossRef]
54. Parr, R.G.; Yang, W. *Density-Functional Theory of Atoms and Molecules*; Oxford University Press: Oxford, UK, 1989.
55. Frisch, M.J.; Trucks, G.W.; Schlegel, H.B.; Scuseria, G.E.; Robb, M.A.; Cheeseman, J.R.; Zakrzewski, V.G.; Montgomery, J.A.; Stratmann, R.E.; Burant, J.C.; et al. *Gaussian 16, Revision C.01*; Gaussian, Inc.: Wallingford, CT, USA, 2016.

56. Roth, D.; Sadeghi, M. On the computational methods for predicting the potential energy surface of molecular systems. *J. Chem. Phys.* **2020**, *153*, 1–12.
57. Pople, J.A.; Gordon, M.S. *Ab Initio Methods in Quantum Chemistry I: The Hartree-Fock Approach*; Academic Press: Cambridge, MA, USA, 2001.
58. Harris, J.G.; Jones, R.O. Density functional theory: The essentials. *Comput. Mater. Sci.* **2008**, *44*, 348–357. [CrossRef]
59. Schlegel, H.B. Optimization methods. *Wiley Interdiscip. Rev. Comput. Mol. Sci.* **2008**, *2*, 1–20. [CrossRef]
60. Borguet, E.; Osborn, S.B.E.; Ramàöârez, D.J.A.; Toomey, M.J. Potential energy surfaces of transition metal oxides: Methods and models. *J. Phys. Chem. C* **2017**, *121*, 4876–4884. [CrossRef]
61. Nørskov, J.K.; Bligaard, T.; Rossmeisl, J.; Christensen, C.H. Towards the computational design of solid catalysts. *Nat. Chem.* **2009**, *1*, 37–46. [CrossRef] [PubMed]
62. Burkholder, D.J.; McCurdy, W.R.; Linehan, M.S. GENCEP: A generalized electronically contracted pseudoatom basis set for modeling transition metal compounds. *J. Chem. Theory Comput.* **2006**, *2*, 1384–1390. [CrossRef]
63. Dennis, J.E.; Schnabel, R.B. *Numerical Methods for Unconstrained Optimization and Nonlinear Equations*; SIAM: Philadelphia, PA, USA, 1996.
64. LeCun, Y.; Bengio, Y.; Hinton, G. Deep learning. *Nature* **2015**, *521*, 436–444. [CrossRef]
65. Amodei, D.; Ananthanarayanan, S.; Anubhai, R.; Bai, J.; Battenberg, E.; Bell, J.; Case, C.; Casper, J.; Catanzaro, B.; Cheng, Q. Deep speech 2: End-to-end speech recognition in English and Mandarin. In Proceedings of the 33rd International Conference on Machine Learning (ICML), New York, NY, USA, 19–24 June 2016; Volume 2, pp. 173–182.
66. Cheng, F.; Sun, Y.; Zhao, Y.; Song, M.; Wang, J. Deep learning-based feature engineering methods for improved building energy prediction. *Appl. Energy* **2019**, *240*, 35–45.
67. Karpathy, A.; Toderici, G.; Shetty, S.; Leung, T.; Sukthankar, R.; Fei-Fei, L. Large-scale video classification with convolutional neural networks. In Proceedings of the IEEE Conference on Computer Vision and Pattern Recognition (CVPR), Columbus, OH, USA, 23–28 June 2014; pp. 1725–1732.
68. Perdew, J.P.; Burke, K.; Ernzerhof, M. Generalized gradient approximation made simple. *Phys. Rev. Lett.* **1996**, *77*, 3865–3868. [CrossRef]
69. Liu, S.; Zhao, D.; Gao, X.; Li, J. Mapping the energy profile of catalytic reactions: The importance of Potential Energy Surface (PES) calculations. *J. Catal.* **2019**, *370*, 98–107. [CrossRef]
70. Johnston-Haynes, E. Reference Electrode Development in Polymer Electrolyte Membrane (PEM) Electrolyzer Assembly for Novel Investigation of Electrodes. Ph.D. Thesis, Queen's University, Kingston, ON, Canada, 2018.
71. Yang, L.; Liu, C. Computational exploration of transition metal oxides for electrocatalysis: Insights from DFT calculations and the CHAMP database. *Catal. Sci. Technol.* **2020**, *10*, 2400–2412.
72. Steckel, J.A.; Sholl, D. *Density Functional Theory: A Practical 673 Introduction*; Wiley: Hoboken, NJ, USA, 2009.
73. Greeley, J.; Mavrikakis, M.; Norskov, J.K. A density functional theory study of the electronic structure of IrO acitivity surfaces. *J. Phys. Chem. B* **2002**, *106*, 2917–2926. [CrossRef]
74. He, J.; Xie, J.; Zhang, Y.; Yang, X.; Wei, Z.; Liu, Q.; Yao, T.; Yang, X.; Zhang, L.; Liu, B.; et al. Electronic Structure of IrO_2 and Its Role in the Oxygen Evolution Reaction. *Nat. Commun.* **2017**, *8*, 237.
75. The Materials Project. *Materials Data on IrO2 by Materials Project*; Lawrence Berkeley National Laboratory (LBNL): Berkeley, CA, USA, 2020. [CrossRef]
76. Minenkov, Y.; Singstad, Å.; Occhipinti, G.; Jensen, V.R. The accuracy of DFT-optimized geometries of functional transition metal compounds: A validation study of catalysts for olefin metathesis and other reactions in the homogeneous phase. *Dalton Trans.* **2012**, *41*, 5526–5541. [CrossRef]
77. Ping, Y.; Galli, G.; Goddard, W.A. Electronic structure of IrO_2: The role of the metal d orbitals. *J. Phys. Chem. C* **2015**, *119*, 11570–11577. [CrossRef]
78. Huynh-Thu, V.A.; Saeys, Y.; Wehenkel, L.; Geurts, P. Statistical interpretation of machine learning-based feature importance scores for biomarker discovery. *Bioinformatics* **2012**, *28*, 1766–1774. [CrossRef] [PubMed]
79. Yang, W.; Yi, J.; Sun, W.-H. Revisiting benzylidenequinolinylnickel catalysts through the electronic effects on catalytic activity by DFT studies. *Macromol. Chem. Phys.* **2015**, *216*, 1125–1133. [CrossRef]
80. Cieslak, M.C.; Castelfranco, A.M.; Roncalli, V.; Lenz, P.H.; Hartline, D.K. t-Distributed Stochastic Neighbor Embedding (t-SNE): 781 A tool for eco-physiological transcriptomic analysis. *Mar. Genom.* **2020**, *51*, 100723. [CrossRef] [PubMed]
81. Marcus, R.A. Electron Transfer Reactions in Chemistry, Annual Review of Physical Chemistry. In *Protein Electron Transfer*; Taylor & Francis: Abingdon, UK, 1996; Volume 44, pp. 155–172.
82. Rees, T.A.; Jones, R.E. Charge Transfer in Transition Metal Oxides. *J. Chem. Phys.* **1999**, *110*, 4200–4212.

83. Frisch, M.J.; Trucks, G.W.; Schlegel, H.B.; Scuseria, G.E.; Robb, M.A.; Cheeseman, J.R.; Scalmani, G.; Barone, V.; Mennucci, B.; Petersson, G.A.; et al. *Gaussian 09, Revision E.01*; Gaussian, Inc.: Wallingford, CT, USA, 2016.
84. Duthie, A.M.; Lai, Y.-J.; Hwang, B.-J.; Koper, M.T.M.; van der Maas, J.H.; Strasser, P. Electronic Properties of Iridium Oxide Catalysts for Water Splitting. *Nat. Commun.* **2020**, *11*, 1433.